JACS
JOURNAL OF THE AMERICAN CHEMICAL SOCIETY
Article
pubs.acs.org/JACS

Nanoscale Control of Polymer Assembly on a Synthetic Catalyst−Bilayer System

Ricardo M. Gorgoll, Koji Harano,* and Eiichi Nakamura*

Department of Chemistry, The University of Tokyo, 7-3-1 Hongo, Bunkyo-ku, Tokyo 113-0033, Japan

Supporting Information

ABSTRACT: The use of the interior of self-assembled membrane as a template for polymer synthesis and assembly has long attracted the interest of chemists. However, it is difficult to utilize a lipid membrane as a chemical reactor for controlled assembly for polymers because lipid membrane is easily destabilized by loading of extraneous molecules. We found that a several-nanometer-thick bilayer vesicle made by self-assembly of an organic fullerene amphiphile doped with a metathesis catalyst serves as a nanosized chemical reactor in water, where a polymer is synthesized and assembled, depending on the affinity of the growing polymer to the organic groups on the amphiphile. This catalyst−bilayer system can thus control supramolecular assembly of the ester-functionalized polymer product into different nanoscale structures: a nanoparticle made of a single polymer chain and a nanocapsule made of several tens of polymer chains.

INTRODUCTION

Preparation of nanostructured polymer materials templated by self-assembled scaffolds has long been inspired by biosynthetic machinery on cell membranes,[1−3] but it still remains a challenging subject of research in laboratories.[4−9] Noticing that one of the fundamental problems in this challenge is the excessive fluidity of a lipid or lipid-mimetic membrane,[10,11] we conjectured on the use of a self-assembled bilayer made of an anionic fullerene amphiphile[12] (Figure 1a; **1**−**4**; R = $^{n}C_8F_{17}$, $^{n}C_8H_{17}$, $^{n}C_{20}H_{41}$, H), from which an aqueous solution of a vesicle of a uniform size (typically 30 nm in diameter) is formed spontaneously upon dissolution in water (**V1**−**V4**, respectively).[13] The fullerene bilayer keeps the hydrophilic fullerene anion inside and exposes the hydrophobic groups to an aqueous environment to create three regions: surface, interior, and fullerene-rich core (Figure 1b, left). Herein we report a catalyst−membrane system where catalyst **7**, doped on the vesicle for ring-opening metathesis polymerization (ROMP), controls the assembly of polymer products from a norbornene diethyl ester (**5a**) in three different ways by the choice of the fluorous vesicle **V1**, the octyl vesicle **V2**, and the eicosanyl vesicle **V3**, depending on the miscibility of the growing polymer to the interior of the bilayer. Thus, the polymerization of **5a** on the fluorous vesicle **V1** occurred heterogeneously on the vesicle surface to afford 6 nm sized spherical particles composed mostly of a single polymer chain. In contrast, polymerization of **5a** on the octyl vesicle **V2** occurred homogeneously near the fullerene core of the bilayer to afford a hollow polymer capsule of 35 nm size composed of 20−30 tightly entangled polymer chains. Polymerization on **V3** occurred in the eicosanyl alkyl environment to afford a soft and sticky capsule. When we polymerized a fluorous ester **5d** instead of the diethyl ester **5a** on the fluorous vesicle **V1**, the reaction afforded a polymer homogeneously distributed in the fluorous membrane because of high affinity between the polymer and the bilayer. The ROMP catalysis is tolerant of functional groups[14] and allowed us also to polymerize halide-containing monomers **5c**, as well as a fluorescent copolymer **6b** made of **5a** and **5b** (19:1 ratio).

RESULTS AND DISCUSSION

Loading of Polymerization Catalyst on Fullerene Vesicles. We doped vesicles **V1**−**V3** with a Hoveyda−Grubbs catalyst bearing a tris[(perfluorooctyl)ethyl]silyl group **7** (Figure 1b)[15,16] by addition of its methylene chloride solution to an aqueous solution of **V1**−**V3** that was formed by spontaneous self-assembly of **1**−**3** in water (0.30 mM).[13] The catalyst **7** in water formed aggregates of average diameter of 204 ± 13 nm (Figure 2a top) as measured by dynamic light scattering (DLS) analysis, and the vesicles **V1**−**V3** and a vesicle made of $Ph_5C_{60}K$ (**V4**, Figure 1a) showed a diameter of 27−31 nm as previously described (black lines in Figure 2a).[12,13] Upon loading of **V1**−**V3** with **7**, the diameter remained largely the same (red lines in Figure 2) increasing only by 10−17% (ca. 200 catalyst molecules/vesicle, calculated from the number of fullerene molecules in a single vesicle,[13] or 2 mol% for monomer **5a**; Figure S7).

A phenyl vesicle **V4**, lacking long side chains, however, failed to fully adsorb the catalyst leaving **7** aggregated separately as shown in Figure 2a bottom. In addition to this DLS analysis, we also identified the catalyst aggregates separately from the vesicles by scanning electron microscopy (SEM) (Figure 2b). For this reason, **V4** was not examined further in the catalysis

Received: May 26, 2016
Published: July 12, 2016

DOI: 10.1021/jacs.6b05414
J. Am. Chem. Soc. 2016, 138, 9675−9681

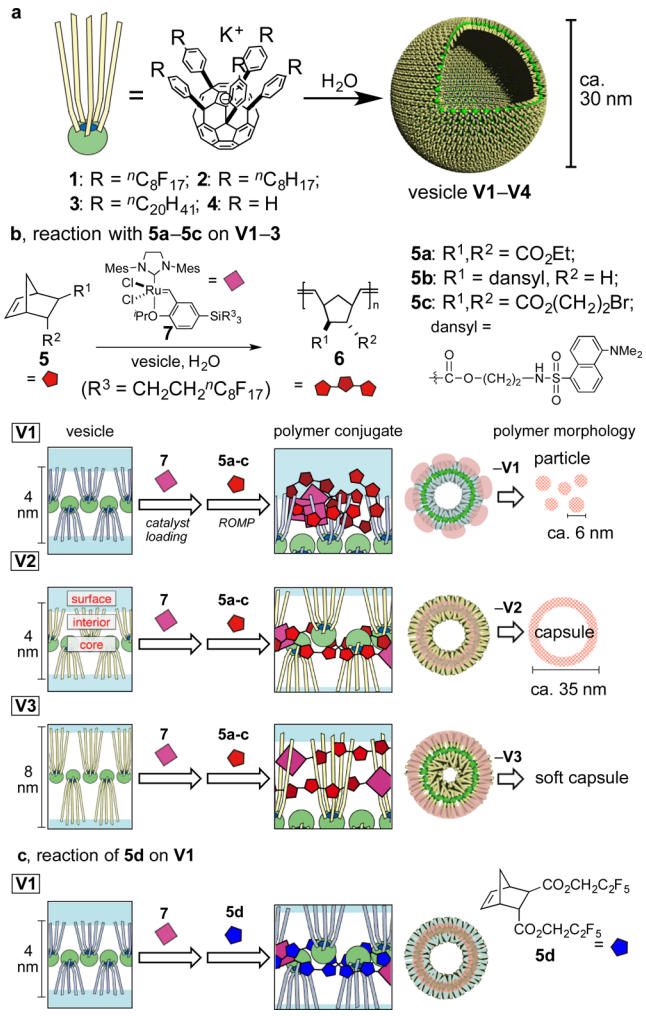

Figure 1. Polymer assembly in a synthetic catalyst–bilayer system. (a) Anionic fullerene amphiphiles **1**–**4** forming a bilayer vesicle (**V1**–**V4**) ca. 30 nm in diameter. (b) Catalyst–bilayer systems made from catalyst molecules **7** and a fullerene bilayer consisting of three different regions: surface, (perfluoro)alkyl-rich interior, and fullerene-rich core. ROMP of **5a**–**5c** produces polymer **6a**–**6c** assembled into three different structures, a robust hollow capsule, a soft capsule, and a single polymer chain particle, after removal of the vesicle template using methylene chloride extraction. (c) Polymerization of a fluorous ester **5d** on **V1** in the interior of the fluorous membrane.

experiments. The contrasting behavior between **V1**–**V3** and **V4** suggests that **V1**–**V3** accommodate the catalyst molecules in their bilayer that is composed of the long side chains. The successful embedment of the catalyst **7** onto **V1**-**V3** is also supported by the vesicle-dependent control of polynorbornene assembly, which is in contrast with the phase-separated catalyst **7** in water that yields ill-defined polymer aggregates (vide infra).

ROMP of Norbornenes 5 on Catalyst-Doped Vesicle. We loaded the doped vesicle with a feedstock for polymerization, the monomer **5a** (water solubility of ca. 14.9 mM),[17] at a monomer/fullerene ratio of 5/1 and monomer/catalyst ratio of 50/1 (2 mol%), and heated the solution at 60 °C for 2 h (>97% conversion). The polymerization process further increased the size of the vesicles by 5–15%. We dissolved the polymer in THF, where the polymer assembly dissociates into a single chain, and measured the molar masses, M_w, by gel permeation chromatography. M_w was determined to be 2.04 × 10^5 (polydispersity index ($Đ$) = 2.11), 2.42 × 10^5 (1.98), and 2.80 × 10^5 (1.87) g mol^{-1} for **V1**, **V2**, and **V3**, respectively. The molar mass of an amorphous polymer obtained in water without the vesicle showed a similar value of 3.33 × 10^5 (1.83) g mol^{-1} (760-mer, suggesting only a small portion of the catalyst molecules were active, perhaps because of aggregation). Given the monomer/fullerene ratio of 5/1 and the average number of vesicles in the solution ((6–10) × 10^{16} L^{-1}), we estimate that each vesicle contains ca. 20–30 polymer chains. We also copolymerized **5a** and a dansyl ester **5b** (95/5) on **V1**–**V3** in the same manner (Figure 1b).

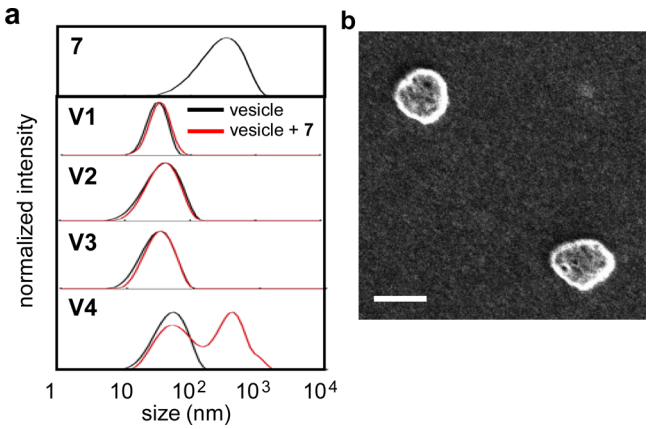

Figure 2. Loading of the catalyst **7** on vesicles **V1**–**V4**. (a) DLS size distribution of the aggregate of **7** (top) and fullerene vesicles **V1**–**V4** in water at 25 °C before (black line) and after catalyst loading (red). (b) SEM images of the aggregates of catalyst **7** on a conductive indium–zinc oxide (IZO)/glass substrate at a landing voltage of 200 V under 10^{-5} Pa. The scale bar is 100 nm.

Growth of Polymer Nanoparticles on V1. We examined the surface morphology of the vesicles after ROMP by low-landing voltage SEM[18] equipped with a monochromator,[19] which we have recently shown to be useful for the structural analysis of organic molecular aggregates placed on a conductive substrate such as IZO.[20–23] As illustrated in Figure 3a, polymerization of the diethyl ester monomer **5a** on the catalyst-doped fluorous vesicle **V1** yielded the polymer **6a** seen as bulges of several nanometers in diameter, suggesting that the polymer product was phase-segregated from the fluorous membrane as ROMP of **5a** progresses.

The polymer bulges on **V1** were extracted with methylene chloride as small spherical objects leaving behind the anionic vesicle in water. The diameter was 5.5 ± 2.9 nm in diameter, as determined by scanning transmission electron microscopy (STEM) (Figure 3b), and supported by the height information obtained by atomic force microscopy (AFM) image in Figure 3d (note that the lateral direction is much overestimated because of the size of a cantilever). In view of the M_w of the polymer (2.04 × 10^5 g mol^{-1}) and its approximate calculated volume, we suggest that the most abundant 5 nm particle (Figure 3c) consists of a single chain of the polymer. The particle diameter, as expected, increased from 4.7 to 5.5 to 24 nm as the catalyst/monomer ratio was decreased from 10 to 2 to 1 mol% (Figure 4). The polymer particles were very robust and maintained their spherical shape after repeated AFM scanning (Figure 3d).

Similarly, ROMP of di(bromoethyl)norbornene dicarboxylate **5c** on **V1** gave the polymer **6c**, which was observed also as bulges on **V1** (Figure 5a) and as particles after extraction with

DOI: 10.1021/jacs.6b05414
J. Am. Chem. Soc. 2016, 138, 9675–9681

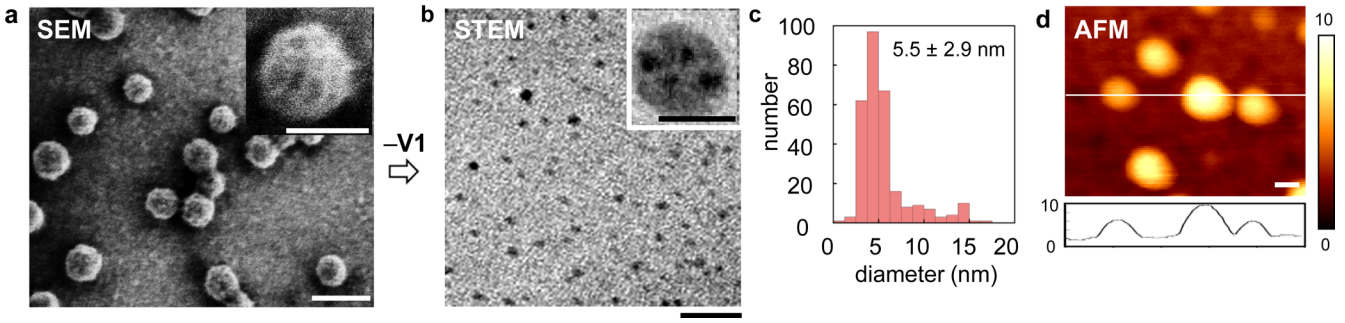

Figure 3. Microscopic analysis of catalyst–vesicle systems made from **V1** doped with 2 mol% catalyst **7**, and morphology of polymer **6a** after methylene chloride extraction of the aqueous solution of polymerization on a vesicle. (a) SEM image of **6a** bulges on **V1** analyzed on an IZO/glass substrate at a landing voltage of 200 V under 10^{-5} Pa. Scale bars are 50 and 20 nm (inset), respectively. (b) STEM image of spherical objects made of **6a** extracted from **V1**. The scale bar is 50 and 10 nm for the inset. In a large particle shown in the inset, we see a few dark spots that are aggregated ruthenium atoms. (c) Histogram of the diameter (STEM) of particles extracted from **V1** + **6a**. (d) AFM image of **6a** on mica after extraction from **V1**. The units of the numbers are nanometers. Scale bar is 50 nm.

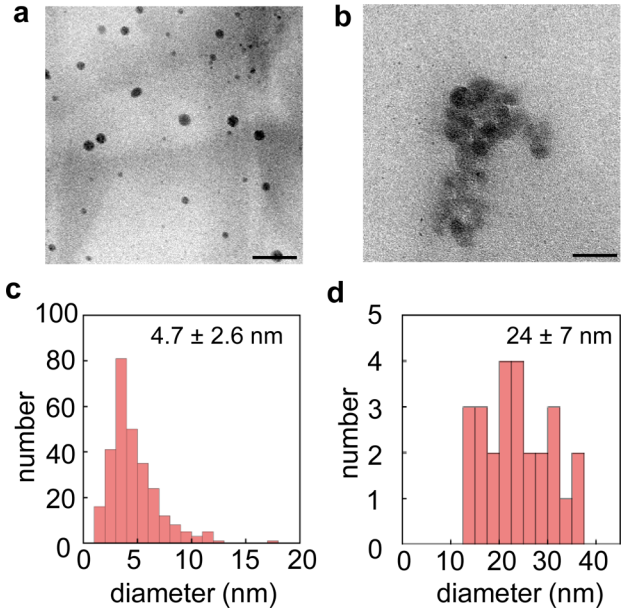

Figure 4. (a,b) STEM images of particles of **6a** obtained from **V1** by using different catalyst/monomer ratios: (a) 10 mol% and (b) 1 mol%. The polymer particles were found as aggregates in image (b). The scale bars are 50 nm. (c,d) Histograms of the size of nanoparticles prepared at (c) 10 mol% and (d) 1 mol% catalyst, showing the formation of much smaller particles with a larger catalyst loading.

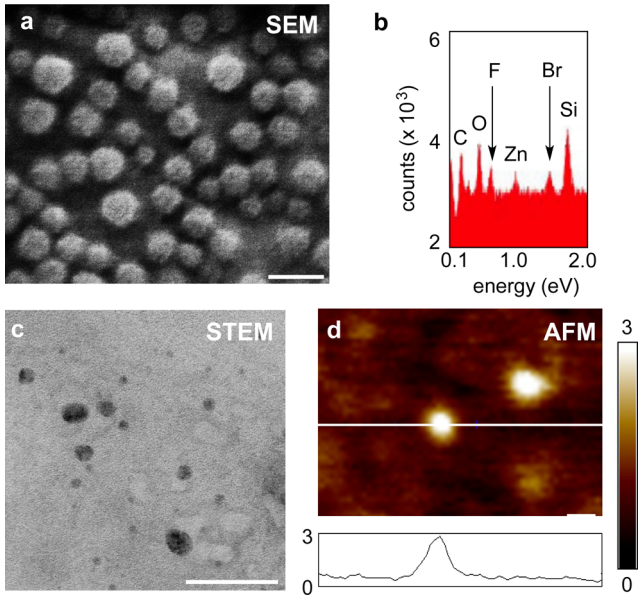

Figure 5. Microscopic analysis of polymer **6c** on **V1**. (a) SEM image **V1** after polymerization of **5c**. Image was obtained on an IZO/glass substrate under a pressure of 10^{-5} Pa. (b) EDX spectrum of **V1** containing **6c**. (c) STEM image of **6c**. The image was obtained on a carbon film substrate under 10^{-5} Pa. Scale bar is 50 nm. (d) AFM image on mica of **6c** after removal of **V1** by dichloromethane extraction. The units of the numbers are nanometers. Scale bar is 50 nm.

methylene chloride by STEM and AFM (Figure 5c,d). Energy dispersive X-ray (EDX) analysis of the polymer–vesicle composite showed expectedly the signals due to carbon, fluorine, and bromine atoms (Figure 5b).

Polymer Assembly into Nanocapsules on V2. We next describe ROMP of the diethyl ester **5a** on **V2** and **V3** doped with catalyst **7**. This reaction allowed the polymer to assemble into a capsule structure. After polymerization of **5a** on **V2**, the surface remained smooth as seen by SEM (Figures 6a and S8), suggesting that the polymer is miscible with the alkyl interior of the membrane and thus homogeneously distributed in the bilayer (Figure 1b, **V2**). The polymer chains of **5a** grew and entangled together tightly in the bilayer, and, interestingly, we were able to isolate the entangled polymer chains as a robust and hollow capsule (Figure 6b) by extraction with methylene chloride (complete removal of fullerene confirmed by UV absorption, Figure S9). Thus, the isolated capsule has a shell thickness of ca. 2 nm (Figure S10) and an average diameter of 35 ± 10 nm (Figure 6c). This diameter agrees with the average of the parent vesicle (30.7 ± 0.6 nm by DLS).

The capsule formed in **V2** was robust enough to be observed by AFM (Figure 6d) as a pancake-like object with an average height of 12.9 ± 3.5 nm, which then collapsed into a ring-like structure after repeated AFM scans (Figures 6e and S11). The polymer capsules showed little tendency to stick to each other. Thus, the capsule is hollow, and the polymer chains in the capsule are tightly entangled together.

The eicosanyl vesicle **V3** doped with **7** has a smooth surface (Figure 2e), and, after the polymerization of **5a**, still has a smooth surface (Figure 6f), indicating that the polymer product is located inside (Figure 1b, **V3**). The polymer assembly isolated by methylene chloride extraction is soft, as seen in

DOI: 10.1021/jacs.6b05414
J. Am. Chem. Soc. 2016, 138, 9675–9681

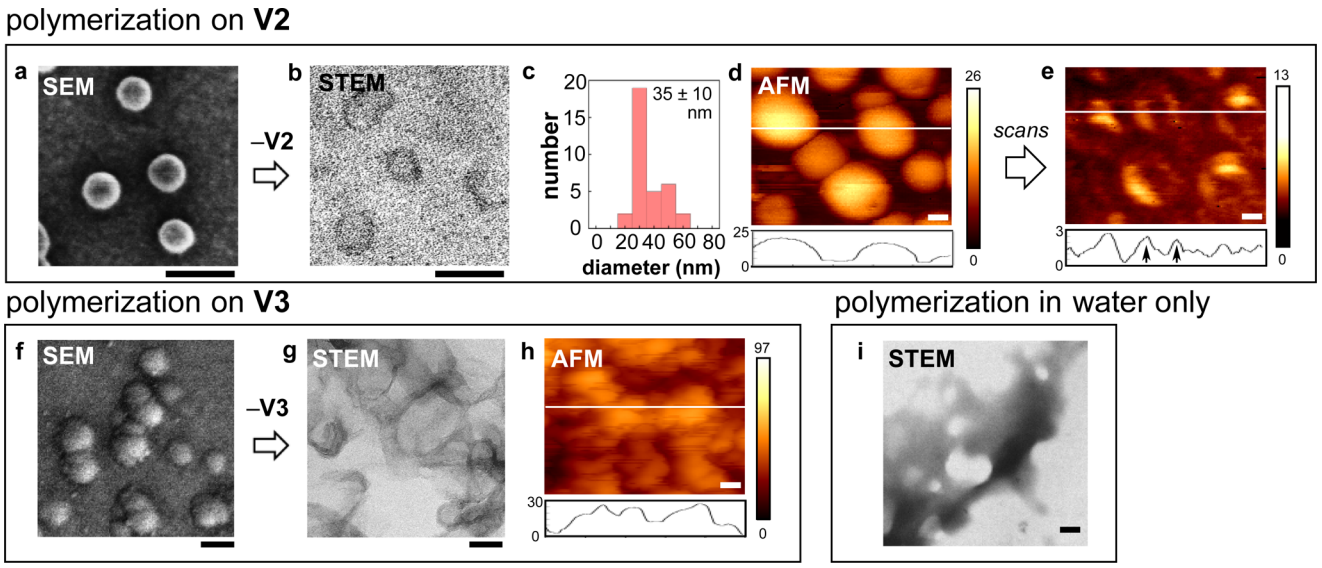

Figure 6. Microscopic analysis of the catalyst–vesicle systems made from **V2** and **V3**, and morphology of polymer **6a** after methylene chloride extraction of the aqueous solution of polymerization. (a) SEM images of **6a** on **V2** taken on an IZO/glass substrate at a landing voltage of 200 V under 10^{-5} Pa. Scale bar is 50 nm. (b) STEM image of structurally defined hollow capsular structure made of **6a** extracted from **V2**. Scale bar is 50 nm. (c) Size distribution of the capsule formed on **V2** as determined by STEM. (d) AFM image of **6a** on mica after methylene chloride extraction from **V2**. A height profile below each AFM image was measured at the white line (height in nm). Scale bar is 50 nm. (e) Collapse of the capsule formed from **V2** after repetitive scans of the polymer capsules shown in d. Scale bar is 50 nm. (f) SEM images of **6a** on **V3** on an IZO/glass substrate at a landing voltage of 200 V under 10^{-5} Pa. Scale bars are 50 nm. (g) STEM image of ill-defined capsular structure made of **6a** extracted from **V3**. Scale bar is 50 nm. (h) AFM image of **6a** on mica after extraction from **V3**. Scale bars are 50 nm. (i) STEM image of **6a** prepared in water without vesicle templates. Scale bar is 50 nm.

STEM and AFM images (Figure 6g,h). We consider that the polymer assembly occurred in the eicosanyl membrane and hence is less tightly entangled than the polymer formed in **V2**. Note that the same polymerization reaction in water in the absence of a vesicle gave an entirely amorphous polymer (Figure 6i).

Fluorescence Study. Fluorescence and water permeation studies supported the microscopic evidence of the polymerization sites in the fullerene bilayer. The fluorescence shift and quenching measurements for the fluorescent copolymer **6b** on **V1**–**V3** gave us the spectroscopic evidence (Figure 7). A red shift of the fluorescence maximum (λ_{max}) of the dansyl dye toward λ_{max} = 550 nm for monomer **5a** in water (black) is a measure of the hydrophilicity of the environment.[24] The λ_{max} value of 471 nm for copolymer **6b** in **V1** (cf. 445 nm for monomer **5b** in perfluorohexane, Figure S12) moved to 525 nm for **6b** in **V3** (cf. 519 nm in methanol). On the other hand, the fluorescence of **6b** in **V2** (red line) was entirely quenched, indicating that the polymer is located in the fullerene core, which is known to be an efficient fluorescence quencher (cf. Figure 1b, top).[25,26] From these data, we conclude that ROMP on **V1** occurred largely in the fluorous region and ROMP on **V3** in the $C_{20}H_{41}$-chain region, while ROMP on **V2** occurred in the fullerene-core region (Figure 1b).

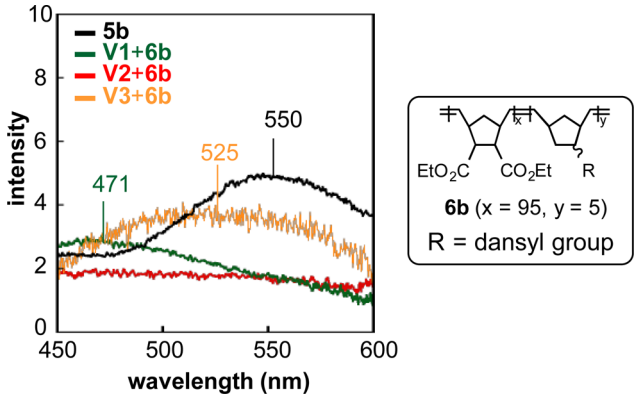

Figure 7. Fluorescence of dansyl copolymer **6b** on the vesicles. Fluorescence spectra (λ_{ex} = 350 nm) of the dansyl group in different environments: monomer **5b** in water (black), **6b** in **V1** (green), **6b** in **V2** (red), and **6b** in **V3** (orange). The concentration of the dansyl group was 1.0 μM.

Water Permeability of Fullerene/Polymer Membrane. The change in the water permeation rate after formation of the ester-functionalized polymer in the bilayer provided additional information. Water permeation is one of the fundamental properties of self-assembled bilayers, and we determined the permeability coefficient of the fullerene membrane by studying the accelerated relaxation of transverse NMR of ^{17}O of water molecules in the vesicle by added paramagnetic Mn^{2+} ion as reported previously.[13,27]

The polymerization made the vesicles uniformly leakier by as much as 12 times for **V2** at 80 °C (black and gray lines; Figure 8a). Interestingly, the reason for the increased water permeation of **V2** was different from that for **V1** and **V3** (Figure 8b), supporting the conclusion in the foregoing paragraph that the polymer in **V2** grew in the core region of the bilayer, while that in **V1** and **V3** grew in the side-chain region. Water permeation through a fullerene bilayer is known to show a very characteristic feature in that the kinetics depend solely on the entropy term (cf. entry "V2" in Figure 8b) because the permeation barrier originates from strong water–fullerene interactions.[27] Water permeation through a lipid bilayer, on the other hand, is controlled largely by ΔH because the liquid-to-gas phase transition of water limits the speed of

DOI: 10.1021/jacs.6b05414
J. Am. Chem. Soc. 2016, 138, 9675–9681

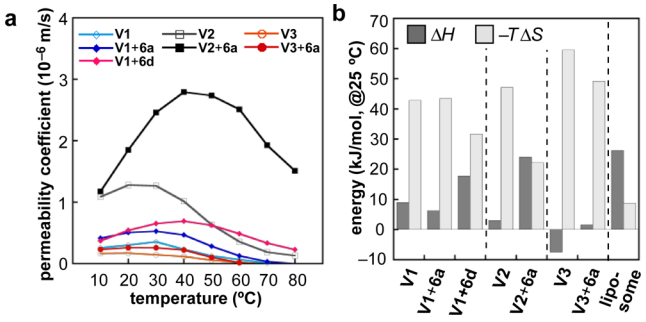

Figure 8. Water permeation profiles of **6a** on **V1**−**V3** and **6d** on **V1**. (a) Temperature dependence of the water permeability coefficient. (b) Activation enthalpy ($\Delta H^{\ddagger}$) and activation entropy ($-T\Delta S^{\ddagger}$) values for water permeation at 25 °C. Data for pristine vesicles **V1**−**V3** were taken from ref 13. Data for a liposome made of a phosphatidylcholine bilayer were taken from ref 27

water permeation (cf. entry "liposome").[28] Therefore, it is notable that the permeation kinetics after ROMP on **V2** becomes controlled by both the enthalpy and the entropy (entry "V2"), suggesting that the fullerene−fullerene network was disturbed by intrusion of polynorbornene chains (cf. Figure 1b, **V1**). In contrast, the water permeation profiles for **V1** and **V3** changed little after polymer formation (cf. entries "V1" vs "V1 + 6a"), indicating that the polynorbornene chains are located in the alkyl and fluoroalkyl regions (cf. Figure 1b, **V2** and **V3**).

ROMP of Fluorous Ester 5d on V1. The contrast between the aliphatic monomer **5a** and the fluorous monomer **5d** upon polymerization on the fluorous vesicle **V1** further illustrates the bilayer control of the polymer morphology (Figure 1c). Thus, ROMP of **5d** on **V1** produced the polymer **6d** homogeneously distributed in the bilayer of **V1** as evidenced by the smooth surface of the polymer/vesicle conjugate (Figure 9), which

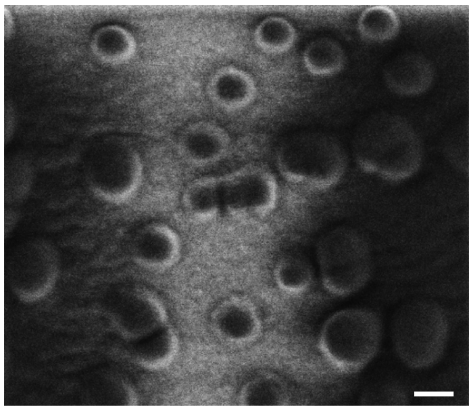

Figure 9. SEM images of composite of fluorous vesicle **V1** and **6d** on an IZO/glass substrate under 10^{-5} Pa. The scale bar is 50 nm.

makes a stark contrast with the bulge formation upon polymerization of **5a** on **V1** (Figure 3a). Water permeation profile of the fluorous/fluorous combination of **V1** + **6d** resembles that of the alkyl/alkyl combination of **V2** + **6a** (Figure 8), further supporting that the fluorous polymer **6d** is miscible with the fluorous side chain of **V1** and is homogeneously located in the interior of **V1**.

CONCLUSION

In summary, we have demonstrated that the fullerene vesicles bearing three different side chains provide different types of nanoscopic reaction sites for **7**-catalyzed ROMP, where the same norbornene diethyl ester **5a** polymerizes and assembles in different ways depending on the nature of the bilayer of the vesicle. In a fluorous bilayer of **V1**, a single polymer chain grows on the membrane surface to assemble into a small nanoparticle. When the polymerization occurs on the octyl vesicle **V2**, polymer chains become tightly assembled together into a shape-persistent hollow capsule. The eicosanyl vesicle **V3**, having the thickest membrane of the three, can only loosely assemble the polymers. The template effect of the bilayer is evident because neither polymerization in the thick membrane of **V3** nor that in the absence of the vesicles provides shape-persistent polymer assemblies after extraction. The present design of the self-assembled membrane scaffold by amphiphilic fullerenes not only supplements the shape control strategy for polymer assembly using lipid vesicles[29−33] but also provides an example of membrane-based synthetic machinery in which chemical reaction and modulation of self-assembled structure of products are achieved simultaneously.[34,35]

EXPERIMENTAL SECTION

Catalyst Loading in the Fullerene Bilayer. A solution of catalyst **7** in dichloromethane (60 μL, 0.500 mM) was added dropwise to an aqueous solution of vesicles (**V1**−**V3**, 1.00 mL, 0.300 mM) while stirring. The solution was stirred for 2 h at 25 °C, and dichloromethane was completely removed before it was used in the polymerization reaction.

General Procedure for Polymerization of 5 in Vesicles Loaded with Catalyst 6. An aqueous solution of fullerene vesicles (0.30 mM, 5.00 mL) loaded with catalyst **7** (fullerene/catalyst ratio of 5) was added to a thin film of diethyl bicyclo[2.2.1]hept-5-ene-2,3-dicarboxylate (**5a**) (monomer/catalyst ratio of 50) prepared from evaporation of a dichloromethane solution (20.0 mM, 375 μL). The reaction mixture was stirred for 2 h at 60 °C. After cooling to room temperature, the aqueous solution was extracted with dichloromethane (3 × 10 mL). Removal of the organic solvent under reduced pressure gave polynorbornene **6a** (2.14−3.50 mg) as a white solid (yield: 60−98%). ^{1}H NMR (400 MHz, $CDCl_3$) δ 1.21−1.32 (m, 6H), 1.37−1.66 (m, 1H), 1.77−2.12 (m, 1H), 2.40−3.40 (m, 4H), 3.98−4.32 (m, 4H), 5.14−5.73 (m, 2H). ^{13}C NMR (100 MHz, $CDCl_3$) δ 14.2−14.3, 39.3−41.7, 44.6−46.6, 51.6−53.4, 60.4−60.8, 129.5−130.5, 132.5−133.6, 172.8−173.9. **6c** (1.43 mg) was obtained from **5c** in the same procedure. Yield: 43%. ^{1}H NMR ($CDCl_3$, 500 MHz) δ 0.70−0.81 (m, 1H), 1.85−2.18 (m, 1H), 2.78−3.81 (m, 8H), 4.37−4.41 (m, 4H), 5.27−5.56 (m, 2H).

Dynamic Light Scattering Analysis. DLS measurements were performed on a Malvern Zetasizer Nano ZS equipped with a He−Ne laser operating at 4 mW power and 633 nm wavelength, and a computer-controlled correlator, at a 173° accumulation angle. Measurements were carried out at 25 °C in a polystyrene or glass cuvette. The data were processed using dispersion technology software version 5.10 to give Z-average particle size and polydispersity index value by cumulant analysis, and particle size distribution by CONTIN analysis.

High-Resolution Scanning Electron Microscopy Observation. An aqueous solution of fullerene vesicles after polymerization of **5a** (0.5 mL) prepared by the procedure described above was deposited on the surface of an IZO/glass substrate treated by UV/O_3 and spin-coated at 500 rpm for 3 s and at 1500 rpm for 30 s. The sample was dried under reduced pressure (10^{-2} Pa) at room temperature for several hours prior to measure. High-resolution SEM observation was performed on a FEI Magellan 400L instrument at 5 × 10^{-5} Pa. The working distance was set to 0.6−2.0 mm. Secondary electrons were collected with a through-lens detector. Observation at a beam landing

DOI: 10.1021/jacs.6b05414
J. Am. Chem. Soc. 2016, 138, 9675−9681

voltage of 200 V was performed using beam deceleration,[19] where 800 V of beam deceleration bias was applied to the primary electron beam accelerated at a voltage of 1 kV.

High-Resolution Scanning Tunneling Electron Microscopy Observation. A dichloromethane solution of **6** (2 μL, 1 μM) was put on a TEM copper mesh coated with carbon film (Super Ultra High Resolution Carbon film, thickness <6 nm, Oken Shoji Co., Ltd.) and then dried under reduced pressure (10^{-2} Pa) at room temperature for several hours prior to measurements. Measurements were carried out on a JEM-2100F with acceleration voltage of 200 kV with a current of 0.5 pA.

Atomic Force Microscopy Observation. AFM measurements were conducted on a JEOL JSPM-4200 instrument with a silicon cantilever (NSC-350, resonant frequency 120−190 kHz) or a Bruker Multimode 8 AFM with a silicon cantilever (ScanAsyst-Air, resonant frequency 45−95 kHz). Samples were deposited on a mica substrate (5×5 mm^2) in aliquot of 2 μL under air. After drying the sample by blowing air for 10 s and under reduced pressure (5×10^{-2} Pa), the AFM images were obtained with AC mode measurement.

Measurement of Water Permeability of Fullerene Vesicles. A 0.50 mM solution of $MnCl_2$ in Milli-Q water (0.25 mL) was added slowly to 0.25 mL of a solution of fullerene vesicle after the polymerization procedure. The hydrodynamic radius of the vesicle was determined by DLS in different temperatures, from 10 to 80 °C in intervals of 10 °C. For the water permeability experiment, 30 μL of 0.50 mM solution of $MnCl_2$ in water containing 20% of $H_2{}^{17}O$ was slowly added to 30 μL of the vesicle solution after polymerization. The sample solution was transferred to an N-502B capillary NMR tube (tube diameter, 2 mm; Nihon Seimitsu Kagaku, Tokyo, Japan). The transverse relaxation time (T_2) of ^{17}O was recorded without spinning the sample tube. The NMR probe temperature was calibrated using methanol (10−30 °C) and ethylene glycol (40−80 °C) before the measurement. We measured the transverse relaxation time of the vesicle solution from 10 to 80 °C in steps of 10 °C. The sample was equilibrated for 5 min at the set temperature each time, and the relaxation time was recorded three times at that temperature.

The transverse relaxation time of the interior water (T_{2i}) was measured, and, as a reference, the transverse relaxation time of blank water (T_{2ref}) also was measured. The permeability coefficient was obtained from eq 1.

$$P = \frac{R}{3}\left(\frac{1}{T_{2i}} - \frac{1}{T_{2ref}}\right) \quad (1)$$

Eyring Analysis of the Water Permeability. Thermodynamic parameters of the water permeability were obtained by the method developed by Eyring.[36] The Eyring equation is shown in eq 2,

$$P = \frac{\lambda^2 kT}{Lh} \exp\left(\frac{\Delta S^{\ddagger}}{R}\right) \exp\left(\frac{\Delta H^{\ddagger}}{RT}\right) \quad (2)$$

where λ is the distance between successive equilibrium positions of permeating species and was assumed to be 0.5 nm, k is the Boltzmann constant, L is the thickness of the membrane, estimated by a molecular model of the membranes, h is the Planck constant, R is the universal gas constant, T is the absolute temperature, $\Delta S^{\ddagger}$ is the entropy of activation for permeation, and $\Delta H^{\ddagger}$ is the enthalpy of activation for permeation.

The permeability coefficients were thus plotted as $\ln(P/T)$ vs $1/T$. A fitted line was obtained from 10−30 °C by least-squares fitting of the above equation to obtain $-\Delta H^{\ddagger}R$ as the slope and $\ln(\lambda^2 k/Lh) + \Delta S^{\ddagger}/R$ as the intercept (Figure S13). The value of λ (the distance between successive equilibrium positions of permeating species) is in the range of 0.3−1.1 nm. The variation in the entropy of activation in this range of λ is ca. ±5%. We assumed λ to be 0.5 nm, following the discussion of Eyring. The thickness of the fullerene membrane (L) is estimated by molecular modeling of fullerene membrane structure.

■ ASSOCIATED CONTENT

Supporting Information

The Supporting Information is available free of charge on the ACS Publications website at DOI: 10.1021/jacs.6b05414.

Additional experimental procedures, methods, microscopic images, and absorption spectra (PDF)

■ AUTHOR INFORMATION

Corresponding Authors

*harano@chem.s.u-tokyo.ac.jp
*nakamura@chem.s.u-tokyo.ac.jp

Notes

The authors declare no competing financial interest.

■ ACKNOWLEDGMENTS

We thank Prof. Kyoko Nozaki, Dr. Shingo Ito, Mr. Takahiro Ohkawara, and Mr. Wenhan Wang (The University of Tokyo) for GPC analysis. We thank Dr. Sai Prakash Maddala (The University of Tokyo) for SEM/EDX analysis. This research is supported by KAKENHI (no. 15H05754 to E.N. and no. 26708016 to K.H., MEXT, Japan) and CREST, JST. R.M.G. thanks the Japan Society for the Promotion of Science for Young Scientists for a Research Fellowship (No. 24-8773).

■ REFERENCES

(1) Alberts, B.; Johnson, A.; Lewis, J.; Raff, M.; Roberts, K.; Walter, P. *Molecular Biology of the Cell*, 5th ed.; Garland Science: New York, 2008.

(2) van Meer, G.; Voelker, D. R.; Feigenson, G. W. *Nat. Rev. Mol. Cell Biol.* **2008**, *9*, 112−124.

(3) Bogdanov, M.; Dowhan, W. *J. Biol. Chem.* **1999**, *274*, 36827−36830.

(4) Vriezema, D. M.; Comellas Aragonès, M.; Elemans, J. A. A. W.; Cornelissen, J. J. L. M.; Rowan, A. E.; Nolte, R. J. M. *Chem. Rev.* **2005**, *105*, 1445−1490.

(5) Rosen, B. M.; Wilson, C. J.; Wilson, D. A.; Peterca, M.; Imam, M. R.; Percec, V. *Chem. Rev.* **2009**, *109*, 6275−6540.

(6) Himmelein, S.; Ravoo, B. J. In *Bioinspiration and Biomimicry in Chemistry: Reverse-Engineering Nature*, 1st ed.; Swiegers, G. F., Ed.; Wiley: New York, 2012; Chap. 8.

(7) Miyako, E.; Kono, K.; Yuba, E.; Hosokawa, C.; Nagai, H.; Hagihara, Y. *Nat. Commun.* **2012**, *3*, 1226.

(8) Kurihara, K.; Tamura, M.; Shohda, K.-I.; Toyota, T.; Suzuki, K.; Sugawara, T. *Nat. Chem.* **2011**, *3*, 775−781.

(9) Krause, J. O.; Zarka, M. T.; Anders, U.; Weberskirch, R.; Nuyken, O.; Buchmeiser, M. R. *Angew. Chem., Int. Ed.* **2003**, *42*, 5965−5969.

(10) Cullis, P. R.; De Kruijff, B. *Biochim. Biophys. Acta, Rev. Biomembr.* **1979**, *559*, 399−420.

(11) Rosoff, M., Ed. *Vesicles*; Marcel Dekker: New York, 1996.

(12) Zhou, S. Q.; Burger, C.; Chu, B.; Sawamura, M.; Nagahama, N.; Toganoh, M.; Hackler, U. E.; Isobe, H.; Nakamura, E. *Science* **2001**, *291*, 1944−1947.

(13) Homma, T.; Harano, K.; Isobe, H.; Nakamura, E. *J. Am. Chem. Soc.* **2011**, *133*, 6364−6370.

(14) Dubois, P., Coulembier, O., Raquez, J.-M., Eds. *Handbook of ring-opening polymerization*; Wiley-VCH: Weinhemi, 2009.

(15) Michalek, F.; Bannwarth, W. *Helv. Chim. Acta* **2006**, *89*, 1030−1037.

(16) Hensle, E. M.; Tobis, J.; Tiller, J. C.; Bannwarth, W. *J. Fluorine Chem.* **2008**, *129*, 968−973.

(17) Svirbely, W. J.; Eareckson, W. M.; Matsuda, K.; Pickard, H. B.; Solet, I. S.; Tuemmler, W. B. *J. Am. Chem. Soc.* **1949**, *71*, 507−509.

(18) Roussel, L. Y.; Stokes, D. J.; Gestmann, I.; Darus, M.; Young, R. J. *Proc. SPIE* **2009**, 73780W.

DOI: 10.1021/jacs.6b05414
J. Am. Chem. Soc. 2016, 138, 9675−9681

(19) Young, R.; Henstra, S.; Chmelik, J.; Dingle, T.; Mangnus, A.; van Veen, G.; Gestmann, I. *Proc. SPIE* **2009**, 737803.
(20) Harano, K.; Okada, S.; Furukawa, S.; Tanaka, H.; Nakamura, E. *J. Polym. Sci., Part B: Polym. Phys.* **2014**, *52*, 833−841.
(21) Yabu, H.; Kanahara, M.; Shimomura, M.; Arita, T.; Harano, K.; Nakamura, E.; Higuchi, T.; Jinnai, H. *ACS Appl. Mater. Interfaces* **2013**, *5*, 3262−3266.
(22) Harano, K.; Yamada, J.; Mizuno, S.; Nakamura, E. *Chem. - Asian J.* **2015**, *10*, 172−176.
(23) Harano, K.; Minami, K.; Noiri, E.; Okamoto, K.; Nakamura, E. *Chem. Commun.* **2013**, *49*, 3525−3527.
(24) Holmes-Farley, S. R.; Whitesides, G. M. *Langmuir* **1986**, *2*, 266−281.
(25) Harano, K.; Gorgoll, R. M.; Nakamura, E. *Chem. Commun.* **2013**, *49*, 7629−7631.
(26) Matsuo, Y.; Morita, K.; Nakamura, E. *Chem. - Asian J.* **2008**, *3*, 1350−1357.
(27) Isobe, H.; Homma, T.; Nakamura, E. *Proc. Natl. Acad. Sci. U. S. A.* **2007**, *104*, 14895−14898.
(28) Reeves, J. P.; Dowben, R. M. *J. Membr. Biol.* **1970**, *3*, 123−141.
(29) Meier, W. *Chem. Soc. Rev.* **2000**, *29*, 295−303.
(30) Dergunov, S. A.; Kesterson, K.; Li, W.; Wang, Z.; Pinkhassik, E. *Macromolecules* **2010**, *43*, 7785−7792.
(31) Jarroux, N.; Keller, P.; Mingotaud, A.-F.; Mingotaud, C.; Sykes, C. *J. Am. Chem. Soc.* **2004**, *126*, 15958−15959.
(32) Hentze, H.-P.; Kaler, E. W. *Curr. Opin. Colloid Interface Sci.* **2003**, *8*, 164−178.
(33) Gomes, J. F. P. D. S.; Sonnen, A. F. P.; Kronenberger, A.; Fritz, J.; Coelho, M. Á. N.; Fournier, D.; Fournier-Nöel, C.; Mauzac, M.; Winterhalter, M. *Langmuir* **2006**, *22*, 7755−7759.
(34) Such, G. K.; Johnston, A. P. R.; Caruso, F. *Chem. Soc. Rev.* **2011**, *40*, 19−29.
(35) Kim, D.; Kim, E.; Lee, J.; Hong, S.; Sung, W.; Lim, N.; Park, C. G.; Kim, K. *J. Am. Chem. Soc.* **2010**, *132*, 9908−9919.
(36) Zwolinski, B. J.; Eyring, H.; Reese, C. E. *J. Phys. Colloid Chem.* **1949**, *53*, 1426−1453.

DOI: 10.1021/jacs.6b05414
J. Am. Chem. Soc. 2016, 138, 9675−9681